

Antiferro octupolar order in the $5d^1$ double perovskite $\text{Sr}_2\text{MgReO}_6$ and its spectroscopic signatures

Dario Fiore Mosca¹ and Leonid V. Pourovskii^{2,3}

¹University of Vienna, Faculty of Physics and Center for Computational Materials Science, Vienna, Austria

²CPhT, CNRS, École polytechnique, Institut Polytechnique de Paris, 91120 Palaiseau, France

³Collège de France, Université PSL, 11 place Marcelin Berthelot, 75005 Paris, France

”Hidden”-order phases with high-rank multipolar order parameters have been recently detected in several cubic double perovskites of $5d$ transition metals. Here, by constructing and solving an ab initio low-energy Hamiltonian, we show that an antiferroic order of magnetic octupoles also forms in the tetragonal $5d^1$ double perovskite $\text{Sr}_2\text{MgReO}_6$. The low-temperature order in this material is determined by a tetragonal crystal field dominating over exchange interactions. This results in a well isolated crystal-field doublet ground state hosting octupolar low-energy degrees of freedom. Very weak dipole moments entangled with the primary octupole order parameters are induced by admixture of the excited $j_{1/2}$ spin-orbit multiplet. We show that the octupolar order leads to characteristic quasi-gapless magnetic excitation spectra as well as to the intensity of superstructural neutron diffraction reflexes peaking at large scattering momenta.

Introduction. The importance of the relativistic Spin Orbit (SO) coupling extends across different areas of chemistry and physics. Its effect of entangling spin and orbital degrees of freedom is especially important for the case of correlated insulators, where it is predicted to foster a variety of unconventional and exotic states of matter [1–4]. The family of heavy transition metal oxides falls in this category and it has attracted much interest because of the possibility of realizing exotic low-temperature phases like the elusive Kitaev spin liquid in $5d^5$ Mott insulators [5, 6], or high-rank multipole orders. The latter, which are challenging to detect with conventional experimental probes and thus referred to as *hidden*, have been reported [7–9] in d^1 and d^2 double perovskites (DPs) $A_2BB'\text{O}_6$ (where B' is a heavy magnetic transition metal ion, A and B are non-magnetic cations).

An intensive experimental and theoretical effort has recently been focused on the $5d^1$ DPs where the unquenched orbital angular momentum ($l = 1$) produced by the octahedral crystal field (CF) of ligands is coupled through SO to the spin ($S = 1/2$). This SO entanglement results in a total angular momentum $j_{eff} = 3/2$ ground state (GS) multiplet (See Figure 1a), which can host high rank multipoles [3]. Initially, theoretical studies primarily focused on electronic exchange and electrostatic interactions [10–12], suggesting that these mechanisms could drive the ordering of charge quadrupoles without breaking time-reversal symmetry, and subsequently induce a paramagnetic to canted antiferromagnetic phase transition. Experimental investigations of cubic $5d^1$ DPs such as $\text{Ba}_2\text{MgReO}_6$ [9, 13] and $\text{Ba}_2\text{NaOsO}_6$ [8], have confirmed the existence of this two-step phase transition. However, the origin is now largely attributed to either vibronic interactions within the $j_{eff} = 3/2$ ground state multiplet (GSM), which are Jahn-Teller active [14–16], or to their interplay with electronic superexchange interactions [17–19]. While cubic DPs (space group $Fm\bar{3}m$) have attracted considerable interest, other structural variants

have been relatively overlooked, despite their potential to host intriguing unconventional orders. Notably, Chen and coworkers [10] pointed out the possibility of an antiferroic ordering of magnetic octupoles with a “vanishing static magnetic dipole moment” for tetragonal DPs with elongated $B'\text{O}_6$ octahedra (or easy-axis anisotropy). The spin-orbit DPs that exhibit an elongation of the octahedra are, to our knowledge, the following: $\text{Sr}_2\text{MgReO}_6$ (SMRO), $\text{Sr}_2\text{CaReO}_6$, $\text{Sr}_2\text{ZnReO}_6$, and $\text{Sr}_2\text{LiOsO}_6$ [20–24]. Of these four, the ones that keep a tetragonal space group symmetry $I4/m$ down to low temperatures are $\text{Sr}_2\text{LiOsO}_6$ [22] and SMRO [21]. However, both compounds exhibit, concomitantly with the octahedra elongation, an in-plane tilt (see Figure 1b) that was initially suggested to possibly hinder the formation of octupolar phases [10]. In this study, we will focus on SMRO due to a broader range of experimental data available, as will be detailed in the following.

Initial studies on powder samples proposed SMRO to be a spin glass, as inferred from the absence of magnetic reflections in their neutron diffraction experiment, a broad peak in the magnetic susceptibility at ~ 50 K accompanied by a weak bump in the heat capacity and a bifurcated magnetic susceptibility in field cooling and zero-field cooling measurements up to 300 K [20]. In a recent work, Gao and coworkers [25] were able to synthesize a single crystal of SMRO and characterize it with both synchrotron x-ray diffraction, heat capacity and magnetic susceptibility measurements. Their finding is a single second-order phase transition at $T_N \sim 50$ K towards a collinear dipolar antiferromagnetic (AFM) order with $\mathbf{q} = (001)$. The Re L₃ edge x-ray absorption spectrum at ~ 6 K allowed the authors to infer that the magnetic moments lie within the ab plane, but both the crystallographic direction and the magnitude of the ordered magnetic moments are yet to be resolved [25].

In this Letter, we investigate the magnetic phase of SMRO using advanced first-principles calculations, un-

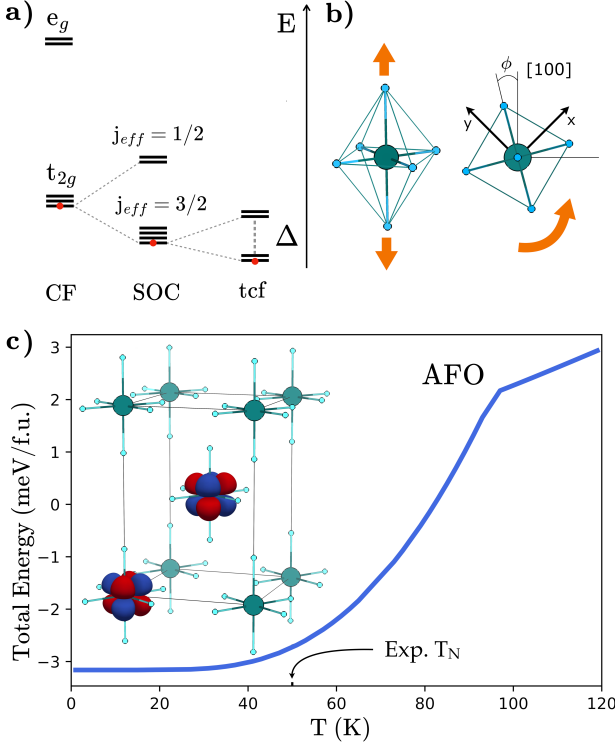


FIG. 1: a) The electronic energy levels of 5d¹ DPs in presence of cubic CF, SOC and tcf. Δ is the $j_{eff} = 3/2$ tcf energy splitting. b) The octahedral distortions present in SMRO: elongation (left) and tilting (right). The angle of tilting ϕ it's defined with respect to the [100] cubic crystallographic axis, rotated by 45° in our unit cell with respect to the global reference frame. c) Mean-field ordering energy vs temperature calculated from eq. 1 for the room temperature structure with $\delta = c/(\sqrt{2}a) - 1 = 6.6 \times 10^{-3}$. The inset shows the antiferro octupolar ordering of $O_{\Gamma_5,y}^3$ alone for clarity.

covering a hidden anti-ferro $\mathbf{q} = (001)$ order of magnetic octupoles (AFO). The formation of the AFO order is induced by a strong tetragonal crystal-field splitting of the $j_{eff} = 3/2$ ground state leading to a well-isolated GS doublet hosting planar octupolar moments. We fully characterize the AFO ordering, analyzing the role of the tetragonal crystal field and the in-plane tilting of the octahedra in its stabilization. Our calculations also predict that mixing between the $j_{eff} = 3/2$ states and excited SO $j_{eff} = 1/2$ doublet induces weak dipolar moments entangled with the leading octupolar order parameters. Furthermore, we identify unambiguous signatures of the AFO order in elastic and inelastic neutron scattering. The AFO order is predicted, in contrast to a conventional $\mathbf{q} = (001)$ dipole order, to feature weak superstructural Bragg peaks with intensity peaked at large Q -vectors and a quasi-gapless magnetic excitation spectrum.

Effective Hamiltonian. The structure of SMRO ex-

hibits tetragonal symmetry at room temperature. As a result, the tetragonal crystal field (tcf) lifts the degeneracy of the $j_{eff} = 3/2$ GSM promoting the $m_j = \pm 3/2$ ($m_J = \pm 1/2$) states if an elongation (compression) of the unit cell appears (See Figure 1 a). While recent experimental and theoretical results propose that vibronic interactions remain active despite the non-cubic symmetry of the system [26], it is questionable whether they play a role in the magnetic properties.

The many-body effective Hamiltonian employed for our study of SMRO incorporates both the electron-mediated intersite exchange interactions (IEI) and the tcf term. The IEI Hamiltonian, which describes the interactions between multipolar moments with a defined total angular momentum $j_{eff} = 3/2$, is expressed within the framework of this effective Hamiltonian, as

$$H_{\text{eff}} = \sum_{\langle ij \rangle} \sum_{\Gamma, \gamma, \Gamma', \gamma'} V_{\Gamma\Gamma', \gamma\gamma'}^{KK'}(ij) O_{\Gamma\gamma}^K(i) O_{\Gamma'\gamma'}^{K'}(j) + \sum_i H_{\text{tcf}}^i, \quad (1)$$

where the first summation $\langle ij \rangle$ runs over the Re-Re bonds, the second summation over the multipolar momenta of the ranks $K, K' = 1, 2, 3$ and irreducible representation (IREP) Γ with projections γ . $O_{\Gamma\gamma}^K(i)$ are the normalized multipolar operators of the rank K , IREP Γ and projection γ acting on the Re site i [3, 27]. $V_{\Gamma\Gamma', \gamma\gamma'}^{KK'}(ij)$ represents the corresponding IEI. We explicitly include the tcf term $H_{\text{tcf}}^i = V_{\text{tcf}} O_{\Gamma_3,z^2}^2$.

Methods. We first calculate the paramagnetic electronic structure of SMRO using the charge self-consistent density functional theory (DFT)[28] + dynamical mean-field theory [29–32] within the quasi-atomic Hubbard-I (HI) approximation [33]. We then determine the multipolar IEI in Eq.1 using the force-theorem in Hubbard-I (FT-HI) approach of Ref. [34]. We employ the FT-HI implementation provided by the publicly available MagInt code, which enables IEI computation for general lattice structures containing multiple correlated sites [35]. See the Supplementary Material (SM) [36]) for further details.

We use the tetragonally distorted room temperature structure of SMRO from ref. [25] with $a = 5.578$ Å, $c = 7.941$ Å. Our DFT+HI calculations correctly reproduce the Re⁶⁺ ground state multiplet $j_{eff} = 3/2$, with tcf splitting $\Delta \approx 28$ meV (See also Figure 1 a). The SO splitting between $j_{eff} = 3/2$ and $j_{eff} = 1/2$ states is ≈ 0.48 eV, in good agreement with the experimental value of 0.53 eV from ref. [26], and the $t_{2g} - e_g$ CF splitting is ≈ 4.6 eV. Following the previous works [17], and in contrast to other proposed approaches for 5d¹ DPs [37–39], we restrict the IEIs to the $j_{eff} = 3/2$ manifold. This is justified by the fact that the strongest calculated $V_{\Gamma\Gamma', \gamma\gamma'}^{KK'}(ij)$ (listed in Supplementary Material, SM [36]) is of about 4 meV \ll SOC splitting. The largest IEI values are also considerably smaller than Δ , implying that the

ordered phase will be governed by the IEI acting within the ground-state doublet $m_J = \pm 3/2$.

This low-lying GSM can therefore be encoded by spin-1/2 operators τ_α , with the states corresponding to the projections of pseudo-spin-1/2. The resulting pseudo-spin Hamiltonian

$$H = \sum_{\langle ij \rangle} \sum_{\alpha\beta} J_{\alpha\beta}(ij) \tau_\alpha(i) \tau_\beta(j), \quad (2)$$

is eq. 1 downfolded into the $m_J = \pm 3/2$ space. Up to a normalization factor, τ_x is a combination of $O_{\Gamma_4,x}^3$ and $O_{\Gamma_5,x}^3$, τ_y is a combination of $O_{\Gamma_4,y}^3$ and $O_{\Gamma_5,y}^3$ and τ_z is a combination of $O_{\Gamma_4,z}^3$ and dipole $O_{\Gamma_4,z}^1$ (See SM for the derivation of the reduced Hamiltonian [36]). Overall, the ordering within this low-energy τ space arises from the competition between purely octupolar operators (τ_x, τ_y) and the mixed dipole-octupole τ_z . The final IEI pseudo-spin matrix for lattice vectors in the ab plane ($[1/2, 1/2, 0]$) and ac plane ($[1/2, 0, 1/2]$) are given in Table I.

We find that the interactions within the ab plane are an order of magnitude weaker than those in the ac and bc planes. This is a consequence of the positive single ion anisotropy induced by the tcf, which promotes xz and yz orbital occupations. The strongest interactions are J_{xx} and J_{yy} , which are identical in the ab plane and differ only slightly for the out-of-plane bonds. Their positive signs indicate an antiferromagnetic coupling between $O_{\Gamma_4,x}^3, O_{\Gamma_5,x}^3$ and $O_{\Gamma_4,y}^3, O_{\Gamma_5,y}^3$ octupoles respectively. The interaction matrices are seen to almost exactly obey the U(1) symmetry as expected at the large tcf limit [10].

Ordered phase. Next, we solve the Eq. 1 within a single-site mean field (MF) using the "McPhase" package [40] together with an in-house module. Care should be exercised in evaluating the realistic magnetic moment of the SMRO $j_{eff} = 3/2$ shell. The quasi-atomic approximation leads to the gyromagnetic factor $g_J = 0$ due to a perfect cancellation of its spin and orbital moments. This cancellation does not occur in real SMRO, which exhibits the effective Curie-Weiss moment of $0.8 \mu_B/f.u.$ corresponding to $g_J=0.413$ [25]. The non-zero magnetic moments of d^1 DPs can be explained by covalency of $5d$ -O-p bonds reducing the $5d$ orbital magnetization [41, 42]. We, correspondingly, employ the experimental g_J that

TABLE I: Calculated IEI downfolded into the $m_J = \pm 3/2$ manifold for the in-plane and out-of-plane Re-Re bonds (in meV).

$\mathbf{R} = [0.5, 0.5, 0]$			$\mathbf{R} = [0.5, 0, 0.5]$				
x	y	z	x	y	z		
x	0.55	0	0	x	4.48	0	0.05
y	0	0.55	0	y	0	4.51	-0.09
z	0	0	0.45	z	0.05	-0.09	2.73

corresponds to the covalency factor $\gamma = 1 - 3g_J/2=0.38$ to compute MF magnetic moments.

We find that SMRO undergoes a single second-order phase transitions at temperature $T_N \approx 92$ K into an AFO order with the propagation wave vector $\mathbf{q} = [0, 0, 1]$ and an octupolar order parameter (OP) that is a mixture of four octupoles (See Figure 1 c). These octupole moments have the following magnitudes: $\langle O_{\Gamma_4,y}^3 \rangle \approx 0.54$, $\langle O_{\Gamma_5,y}^3 \rangle \approx 0.42$, $\langle O_{\Gamma_4,x}^3 \rangle \approx -0.16$ and $\langle O_{\Gamma_5,x}^3 \rangle \approx 0.13$. The calculated Néel temperature is overestimated by $\sim 46\%$ as a consequence of the MF approximation [43–45]. Moreover, our results indicate that this AFO order is *hidden* behind a collinear AFM phase composed of weak dipolar magnetic moments ($\sim 0.06 \mu_B$) with same wave vector and oriented within the ab plane with angle of $\sim 25^\circ$ relative to the x global axis of Figure 1 b.

The dipoles in the AFM phase are not the primary order parameters. They arise directly from the octupolar order for the following reasons: 1) The dipolar MF values are negligible in magnitude compared to the octupolar ones. 2) When computing the magnetic moments M_α with $\alpha = x, y, z$ hosted by the Re $5d$ shell in the saturated $j_{eff} = 3/2$ AFO order with the covalency factor $\gamma = 1$, we find a maximum in-plane moment of $0.16 \mu_B$, with increasing values as the tcf increases (see SM [36] for details).

This seemingly paradoxical result (pure octupoles do not carry a dipole moment) is explained by mixing of the GSM $j_{eff} = 3/2$ with $j_{eff} = 1/2$ states due to the tcf. In result, the octupoles defined within the $j_{eff} = 3/2$ space acquire a small admixture of dipole character upon mapping into physically observable moments of the $5d$ shell. The increase in magnetic moment with increasing tcf further supports this interpretation.

Tilting vs elongation. Early measurements on SMRO and similar systems revealed the emergence of a "glassy state," suggesting that either the tcf was not strong enough to stabilize the octupolar-active GSM or that octahedral tilting played a role in suppressing the AFO phase [10]. To examine this effect, we conducted a series of calculations, systematically varying the tcf through $\delta = c/(\sqrt{2}a) - 1$ and the tilting angle ϕ (see Fig. 1b), while keeping the volume and in-plane Re-O bondlength fixed. The volume constraint is justified by the minimal shrinkage observed across the temperature range ($\sim 0.4\%$ [25]), while the fixed in-plane bond length aligns with experimental findings, which show a significant change in the Re-O(z) bond length while the in-plane bond lengths remain largely unaffected [25].

Our results, summarized in the phase diagram of Figure 2, reveal a region of dipolar canted AFM order, which persists until the tcf produced by the octahedral elongation or tilting angle induce an energy splitting of $\Delta \sim 8$ meV; i.e., when the IEI mean exchange field becomes comparable to the splitting of the $j_{eff} = 3/2$ states. Beyond this threshold, AFO order dominates.

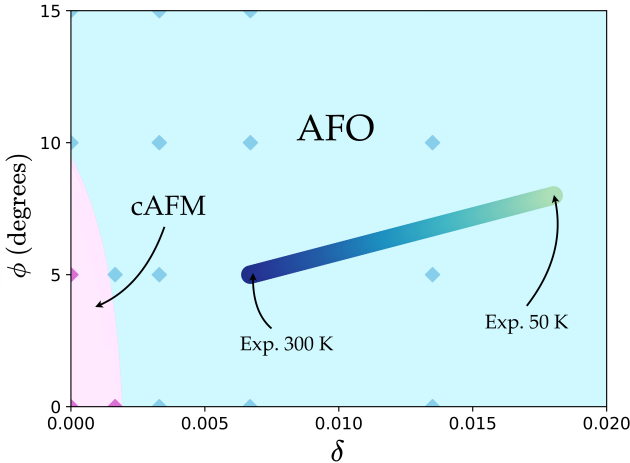


FIG. 2: Phase diagram of SMRO as a function of $\delta = c/(\sqrt{2}a) - 1$ and ϕ (tilting angle). The diamond data-points refer to the actual DFT+HI calculations, while the fading thick line is the "path" in the phase diagram of the SMRO structure as a function of temperature. The Re-O in-plane bondlength has been kept fixed as found experimentally [25].

For comparison, the fading thick line in Fig.2 traces the experimentally observed evolution of the structural parameters. Interestingly, the tilting behaves effectively as a tcf with an exponential scaling (See SM [36]), thus promoting the AFO phase, rather than suppressing it.

Neutron scattering. In order to identify experimental signatures of the predicted octupolar order we have calculated elastic and inelastic neutron scattering in the AFO phase. For the sake of comparison, we have also calculated the same quantities for the hypothetical cAFM phase, which is predicted, as discussed above, to be realized in cubic SMRO.

First, we focus on the magnetic elastic Bragg scattering at the superstructural positions $\mathbf{G} = 2\pi[h/a, k/a, l/c]$, where a and c are the lattice parameters, with $h+k+l = 2n+1$ that are forbidden in the $I4/m$ space group of SMRO. The magnetic Bragg peak intensity reads

$$|F(\mathbf{G})|^2 = \sum_{\alpha\beta} (\delta_{\alpha\beta} - \hat{G}_\alpha \hat{G}_\beta) F_\alpha(\mathbf{G}) F_\beta^*(\mathbf{G}),$$

where $F_\alpha(\mathbf{G}) = \sum_{\mathbf{R}KQ} F_{KQ}^\alpha(\mathbf{G}) \langle O_Q^K \rangle_{\mathbf{R}} \exp\{i\mathbf{GR}\}$ is the structure factor, $\hat{\mathbf{G}} = \mathbf{G}/|G|$, and $\alpha, \beta = x, y, z$ [46]. In the structure factor, $\langle O_Q^K \rangle_{\mathbf{R}}$ is the multipolar order parameter on the sublattice \mathbf{R} in a given ordered phase, $F_{KQ}^\alpha(\mathbf{G})$ is the corresponding neutron scattering form-factor. In order to include the contribution to scattering from octupoles, we calculate the form-factors beyond the dipole approximation for all magnetic multipoles KQ using the approach of Refs. [45, 47]. This method employs the expressions of Ref. [48] to evaluate one-electron

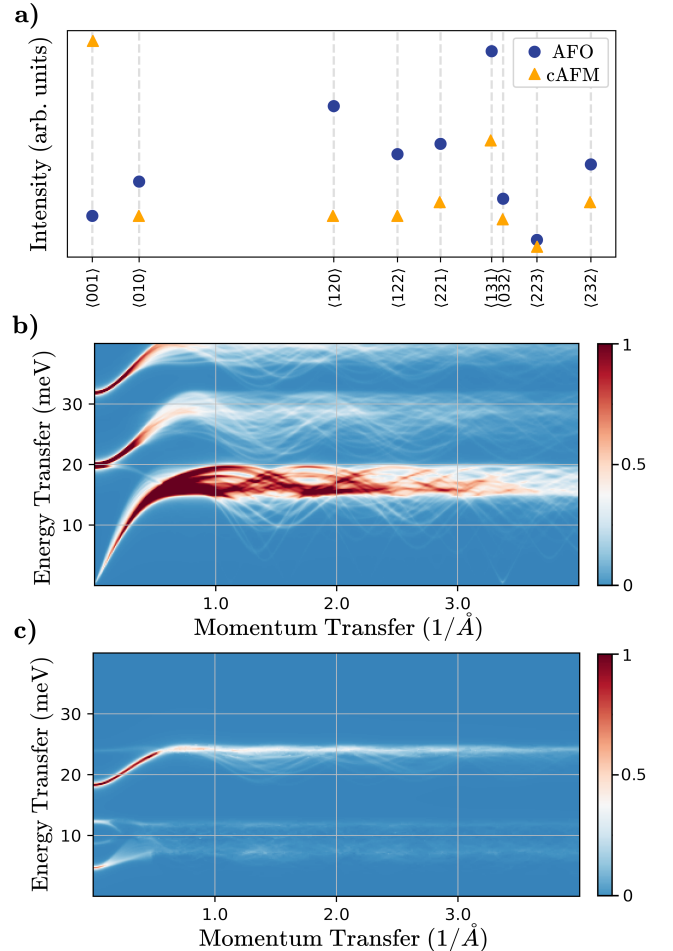


FIG. 3: Neutron scattering in SMRO. a). Calculated intensities of the superstructural peaks $\langle hkl \rangle$ in polycrystalline SMRO in the octupolar AFO and cAFM phases. b). Spherically averaged INS intensity in the AFO phase. c). The same in the cAFM phase.

matrix elements of the spin $\hat{\mathbf{Q}}_s$ and orbital $\hat{\mathbf{Q}}_o$ neutron scattering operators for the $5d$ shell. The resulting matrices are then projected into the $j_{eff} = 3/2$ space and expanded in multipole operators as in the previous application of this method to d^2 DP of Os [45]. To approximately include the effect of covalency on the form-factors we scale down the contribution due to $\hat{\mathbf{Q}}_o$ in the neutron-scattering matrix elements with the experimental covalency factor γ .

The calculated intensities of superstructural peaks are then "powder-averaged" as $\sum_{\{G\}} |F(\mathbf{G})|^2/G^2$, where the sum is over all \mathbf{G} belonging to a given star, to simulate polycrystalline SMRO. The resulting intensities in the AFO phase (Fig. 3a) peak at large \mathbf{G} vectors with the largest magnitude obtained for the $\langle 131 \rangle$ reflection corresponding to $G = 3.65 \text{ \AA}^{-1}$. In contrast, the cAFM intensities exhibit a rapid decay vs G that is typical for magnetic reflections. This remarkable qualitative distinc-

tion between the two phases stems from different behavior of dipole and octupole form-factors, with the former peaked at $G \rightarrow 0$, while the latter reaching maximum magnitudes at finite G of several Å⁻¹.

In Figs 3b and c we display the corresponding inelastic neutron scattering (INS) intensities

$$\sum_{\alpha\beta}(\delta_{\alpha\beta} - \hat{q}_\alpha \hat{q}_\beta) \sum_{\mu\mu'} F_\mu^\alpha(\mathbf{q}) F_{\mu'}^\beta(\mathbf{q}) \text{Im } \chi_{\mu\mu'}(\mathbf{q}, E),$$

where $\chi_{\mu\mu'}(\mathbf{q}, E)$ is the multipolar dynamical susceptibility calculated with the random-phase approximation (RPA)[49], we introduce $\mu \equiv KQ$ for brevity. The form-factors were calculated including the covalency effect as described above, otherwise the approach is the same as in Ref. [45].

The calculated powder-averaged INS intensity in the AFO phase (Fig. 3b) features a bright "acoustic" branch, with a tiny gap of 0.6 meV hardly visible in Fig 3b but clearly resolved by zooming to the region of small q and E [36]. In addition, there are two "optical branches" of lower intensity. Weak quasi-gapless dispersive branches are also observed at finite q values. The quasi-gapless modes stem from the almost exact U(1) symmetry of the projected pseudo-spin-1/2 Hamiltonian (2). The AFO INS spectrum is again drastically different from that of the cAFM phase (Fig. 3c). The latter features a large gap and the higher-energy branch at about 25 meV exhibits the highest intensity.

Conclusions. We have derived the ab initio many-body effective Hamiltonian of SMRO, incorporating both electronic intersite exchange interactions and tetragonal/tilting lattice distortions. Our analysis reveals that intersite exchange interactions are significantly weaker than the induced $j_{eff} = 3/2$ splitting, leading to properties governed primarily by the ground state doublet.

By solving the effective Hamiltonian in the mean-field approximation, we uncover an antiferroic order of octupoles forming in SMRO at temperatures consistent with experimental observations. While this octupolar order was previously predicted at the model level [10], it has never been experimentally observed in a real material. The experimentally inferred collinear dipolar AFM order [25] can thus be interpreted as a "shadow play" with tiny dipole moments both entangled with the primary order octupolar parameters and hiding them.

To characterize this AFO phase and assess its stability, we explore the impact of structural parameters, finding that both tilting and tetragonal distortions play a crucial role in its stabilization with respect to a competing canted antiferromagnetic order of conventional dipole moments. We calculate experimentally observable signatures of the AFO order in elastic and inelastic neutron scattering finding a quasi-gapless magnetic excitation spectrum and a strong enhancement of Bragg superstructural reflections at large q -vectors. Overall, this

study shows how *hidden* magnetic phases can emerge from Kramers' doublet ground states in distorted spin-orbit oxides and provides key insights into their primary driving mechanisms.

Support by the the Austrian Science Fund (FWF) grant J4698 is gratefully acknowledged. D. F. M. thanks the computational facilities of the Vienna Scientific Cluster (VSC). L. V. P. is thankful to the CPHT computer team for support.

-
- [1] W. Witczak-Krempa, G. Chen, Y. B. Kim, and L Balents, "Correlated quantum phenomena in the strong spin-orbit regime," *Annual Review of Condensed Matter Physics* **5**, 57–82 (2014).
 - [2] T. Takayama, J. Chaloupka, A. Smerald, G. Khaliullin, and H. Takagi, "Spin-orbit-entangled electronic phases in 4d and 5d transition-metal compounds," *Journal of the Physical Society of Japan* **90**, 062001 (2021).
 - [3] P. Santini, S. Carretta, G. Amoretti, R. Caciuffo, N. Magnani, and G. H. Lander, "Multipolar interactions in *f*-electron systems: The paradigm of actinide dioxides," *Rev. Mod. Phys.* **81**, 807–863 (2009).
 - [4] Y. Kuramoto, H. Kusunose, and A. Kiss, "Multipole orders and fluctuations in strongly correlated electron systems," *Journal of the Physical Society of Japan* **78**, 072001 (2009).
 - [5] H. Takagi, T. Takayama, G. Jackeli, G. Khaliullin, and S. E. Nagler, "Concept and realization of Kitaev quantum spin liquids," *Nature Reviews Physics* **1**, 264–280 (2019).
 - [6] G. Jackeli and G. Khaliullin, "Mott insulators in the strong spin-orbit coupling limit: From Heisenberg to a quantum compass and Kitaev models," *Phys. Rev. Lett.* **102**, 017205 (2009).
 - [7] D. D. Maharaj, G. Sala, M. B. Stone, E. Kermarrec, C. Ritter, F. Fauth, C. A. Marjerrison, J. E. Greedan, A. Paramekanti, and B. D. Gaulin, "Octupolar versus Néel order in cubic 5d² double perovskites," *Phys. Rev. Lett.* **124**, 087206 (2020).
 - [8] L Lu, M. Song, W. Liu, A. P. Reyes, P. Kuhns, H. O. Lee, I. R. Fisher, and V. F. Mitrović, "Magnetism and local symmetry breaking in a Mott insulator with strong spin orbit interactions," *Nature Communications* **8**, 14407 (2017).
 - [9] D. Hirai, H. Sagayama, S. Gao, H. Ohsumi, G. Chen, T. Arima, and Z. Hiroi, "Detection of multipolar orders in the spin-orbit-coupled 5d Mott insulator Ba₂MgReO₆," *Phys. Rev. Res.* **2**, 022063 (2020).
 - [10] G. Chen, R. Pereira, and L Balents, "Exotic phases induced by strong spin-orbit coupling in ordered double perovskites," *Phys. Rev. B* **82**, 174440 (2010).
 - [11] G. Chen and L Balents, "Spin-orbit coupling in d² ordered double perovskites," *Phys. Rev. B* **84**, 094420 (2011).
 - [12] C. Svoboda, W. Zhang, M. Randeria, and N. Trivedi, "Orbital order drives magnetic order in 5d¹ and 5d² double perovskite Mott insulators," *Phys. Rev. B* **104**, 024437 (2021).
 - [13] D. Hirai and Z. Hiroi, "Successive symmetry breaking in

- a $J_{eff} = 3/2$ quartet in the spin-orbit coupled insulator $\text{Ba}_2\text{MgReO}_6$,” Journal of the Physical Society of Japan **88**, 064712 (2019).
- [14] N Iwahara, V Vieru, and L F. Chibotaru, “Spin-orbital-lattice entangled states in cubic d^1 double perovskites,” Phys. Rev. B **98**, 075138 (2018).
- [15] N. Iwahara and L F. Chibotaru, “Vibronic order and emergent magnetism in cubic d^1 double perovskites,” Phys. Rev. B **107**, L220404 (2023).
- [16] S. Agrestini, F. Borgatti, P. Florio, J. Frassinetti, D. Fiore Mosca, Q. Faure, B. Detlefs, C. J. Sahle, S. Franchoual, J. Choi, M. Garcia-Fernandez, K.-J. Zhou, V. F. Mitrović, P. M. Woodward, G. Ghiringhelli, C. Franchini, F. Boscherini, S. Sanna, and M. Moretti Sala, “Origin of magnetism in a supposedly nonmagnetic osmium oxide,” Phys. Rev. Lett. **133**, 066501 (2024).
- [17] Dario Fiore Mosca, Cesare Franchini, and Leonid V. Pourovskii, “Interplay of superexchange and vibronic effects in the hidden order of $\text{Ba}_2\text{MgReO}_6$ from first principles,” Phys. Rev. B **110**, L201101 (2024).
- [18] D. Fiore Mosca, L V. Pourovskii, B. H. Kim, P. Liu, S. Sanna, F. Boscherini, S. Khmelevskyi, and C. Franchini, “Interplay between multipolar spin interactions, jahn-teller effect, and electronic correlation in a $J_{eff} = \frac{3}{2}$ insulator,” Phys. Rev. B **103**, 104401 (2021).
- [19] J.-R. Soh, M. E. Merkel, L V. Pourovskii, I. Živković, O. Malanyuk, J. Pásztorová, S. Franchoual, D. Hirai, A. Urru, D. Tolj, D. Fiore Mosca, O. Yazyev, N. A. Spaldin, C. Ederer, and H. M. Rønnow, “Spectroscopic signatures and origin of a hidden order in $\text{Ba}_2\text{MgReO}_6$,” (2023), arXiv:2312.01767 [cond-mat.str-el].
- [20] C. R. Wiebe, J. E. Greedan, P. P. Kyriakou, G. M. Luke, J. S. Gardner, A. Fukaya, I. M. Gat-Malureanu, P. L. Russo, A. T. Savici, and Y. J. Uemura, “Frustration-driven spin freezing in the $S=\frac{1}{2}$ fcc perovskite $\text{Sr}_2\text{MgReO}_6$,” Phys. Rev. B **68**, 134410 (2003).
- [21] J E Greedan, Shahab Derakhshan, F Ramezanipour, J Siewenie, and Th Proffen, “A search for disorder in the spin glass double perovskites $\text{Sr}_2\text{CaReO}_6$ and $\text{Sr}_2\text{MgReO}_6$ using neutron diffraction and neutron pair distribution function analysis,” Journal of Physics: Condensed Matter **23**, 164213 (2011).
- [22] V. da Cruz Pinha Barbosa, J. Xiong, P. M. Tran, M. A. McGuire, J. Yan, M. T. Warren, R. V. Aguilar, W. Zhang, M. Randeria, N. Trivedi, D. Haskel, and P. M. Woodward, “The impact of structural distortions on the magnetism of double perovskites containing 5d1 transition-metal ions,” Chemistry of Materials **34**, 1098–1109 (2022).
- [23] H. Kato, T. Okuda, Y. Okimoto, Y. Tomioka, K. Oikawa, T. Kamiyama, and Y. Tokura, “Structural and electronic properties of the ordered double perovskites $A_2\text{MReO}_6$ ($A = \text{Sr}, \text{Ca}$; $M = \text{Mg}, \text{Sc}, \text{Cr}, \text{Mn}, \text{Fe}, \text{Co}, \text{Ni}, \text{Zn}$),” Phys. Rev. B **69**, 184412 (2004).
- [24] María Retuerto, María Jesús Martínez-Lope, Mar García-Hernández, María Teresa Fernández-Díaz, and José Antonio Alonso, “Crystal and magnetic structure of Sr_2MReO_6 ($M = \text{Ni}, \text{Co}, \text{Zn}$) double perovskites: A neutron diffraction study,” European Journal of Inorganic Chemistry **2008**, 588–595 (2008), <https://chemistry-europe.onlinelibrary.wiley.com/doi/pdf/10.1002/ejic.200700753>.
- [25] Shang Gao, Daigorou Hirai, Hajime Sagayama, Hiroyuki Ohsumi, Zenji Hiroi, and Taka-hisa Arima, “Antiferromagnetic long-range order in the $5d^1$ double-perovskite $\text{Sr}_2\text{MgReO}_6$,” Phys. Rev. B **101**, 220412 (2020).
- [26] Felix I. Frontini, Graham H. J. Johnstone, Naoya Iwahara, Pritam Bhattacharyya, Nikolay A. Bogdanov, Liviu Hozoi, Mary H. Upton, Diego M. Casa, Daigorou Hirai, and Young-June Kim, “Spin-orbit-lattice entangled state in $A_2\text{MgReO}_6$ ($A = \text{Ca}, \text{Sr}, \text{Ba}$) revealed by resonant inelastic x-ray scattering,” Phys. Rev. Lett. **133**, 036501 (2024).
- [27] R. Shiina, H. Shiba, and P. Thalmeier, “Magnetic-field effects on quadrupolar ordering in a Γ_8 -quartet system CeB_6 ,” Journal of the Physical Society of Japan **66**, 1741–1755 (1997).
- [28] P Blaha, K Schwarz, G Madsen, D Kvasnicka, J Luitz, R Laskowski, F Tran, and L D. Marks, *WIEN2k, An augmented Plane Wave + Local Orbitals Program for Calculating Crystal Properties* (Karlheinz Schwarz, Techn. Universität Wien, Austria, ISBN 3-9501031-1-2, 2018).
- [29] A. Georges, G. Kotliar, W. Krauth, and M. J. Rozenberg, “Dynamical mean-field theory of strongly correlated fermion systems and the limit of infinite dimensions,” Rev. Mod. Phys. **68**, 13–125 (1996).
- [30] V I Anisimov, A I Poteryaev, M A Korotin, A O Anokhin, and G Kotliar, “First-principles calculations of the electronic structure and spectra of strongly correlated systems: dynamical mean-field theory,” Journal of Physics: Condensed Matter **9**, 7359 (1997).
- [31] A. I. Lichtenstein and M. I. Katsnelson, “Ab initio calculations of quasiparticle band structure in correlated systems: LDA++ approach,” Phys. Rev. B **57**, 6884–6895 (1998).
- [32] M. Aichhorn, L V. Pourovskii, P. Seth, V. Vildosola, M. Zingl, O. E Peil, X. Deng, J. Mravlje, G. J Krabberger, C. Martins, et al., “TRIQS/DFTTools: A TRIQS application for ab initio calculations of correlated materials,” Computer Physics Communications **204**, 200–208 (2016).
- [33] J. Hubbard, “Electron correlations in narrow energy bands,” Proc. Roy. Soc. (London) **A** **276**, 238 (1963).
- [34] L V. Pourovskii, “Two-site fluctuations and multipolar intersite exchange interactions in strongly correlated systems,” Phys. Rev. B **94**, 115117 (2016).
- [35] L. V. Pourovskii and D. Fiore Mosca, “MagInt,” <https://github.com/MagInteract/MagInt>.
- [36] Supplementary Material.
- [37] Wen-Xuan Qiu, Jin-Yu Zou, Ai-Yun Luo, Zhi-Hai Cui, Zhi-Da Song, Jin-Hua Gao, Yi-Lin Wang, and Gang Xu, “Efficient method for prediction of metastable or ground multipolar ordered states and its application in monolayer RuX_3 ($X = \text{Cl}, \text{I}$),” Phys. Rev. Lett. **127**, 147202 (2021).
- [38] S. Y. Zhou, G.-H. Gweon, J. Graf, A. V. Fedorov, C. D. Spataru, R. D. Diehl, Y. Kopelevich, D.-H. Lee, Steven G. Louie, and A. Lanzara, “First direct observation of dirac fermions in graphite,” Nature Physics **2**, 595–599 (2006).
- [39] Yilin Wang, Hongming Weng, Liang Fu, and Xi Dai, “Noncollinear magnetic structure and multipolar order in $\text{Eu}_2\text{Ir}_2\text{O}_7$,” Phys. Rev. Lett. **119**, 187203 (2017).
- [40] M Rotter, “Using mcphase to calculate magnetic phase diagrams of rare earth compounds,” Journal of Magnetism and Magnetic Materials **272-276**, E481–E482 (2004), proceedings of the International Conference on Magnetism (ICM 2003).
- [41] A. Abragam and B. Bleaney, *Electron Paramagnetic Res-*

- onance of Transition Ions*, Oxford Classic Texts in the Physical Sciences (OUP Oxford, 2012).
- [42] Kyo-Hoon Ahn, Karel Pajskr, Kwan-Woo Lee, and Jan Kuneš, “Calculated *g*-factors of 5d double perovskites $\text{Ba}_2\text{NaOsO}_6$ and $\text{Ba}_2\text{YO}_6\text{O}_6$,” Phys. Rev. B **95**, 064416 (2017).
- [43] A. Horvat, L V. Pourovskii, M. Aichhorn, and J. Mravlje, “Theoretical prediction of antiferromagnetism in layered perovskite Sr_2TcO_4 ,” Phys. Rev. B **95**, 205115 (2017).
- [44] L V. Pourovskii and S Khmelevskyi, “Quadrupolar superexchange interactions, multipolar order, and magnetic phase transition in UO_2 ,” Phys. Rev. B **99**, 094439 (2019).
- [45] L V. Pourovskii, D. Fiore Mosca, and C. Franchini, “Ferro-octupolar order and low-energy excitations in d² double perovskites of osmium,” Phys. Rev. Lett. **127**, 237201 (2021).
- [46] We focus on low temperature and thus set the Debye-Weller factor to 1.
- [47] Ryousuke Shiina, Osamu Sakai, and Hiroyuki Shiba, “Magnetic form factor of elastic neutron scattering expected for octupolar phases in $\text{Ce}_{1-x}\text{La}_x\text{B}_6$ and NpO_2 ,” Journal of the Physical Society of Japan **76**, 094702 (2007).
- [48] S. W. Lovesey, “Theory of neutron scattering from condensed matter,” (Clarendon Press, Oxford, 1984) Chap. 11.
- [49] J. Jensen and A. R. Mackintosh, *Rare Earth Magnetism: Structures and Excitations* (Clarendon Press, Oxford, 1991).

Supplementary material for 'Antiferro octupolar order in the 5d¹ double perovskite Sr₂MgReO₆ and its spectroscopic signatures'

Dario Fiore Mosca¹ and Leonid V. Pourovskii^{2,3}

¹University of Vienna, Faculty of Physics and Center for Computational Materials Science, Vienna, Austria

²CPHT, CNRS, École polytechnique, Institut Polytechnique de Paris, 91120 Palaiseau, France

³Collège de France, Université PSL, 11 place Marcelin Berthelot, 75005 Paris, France

(Dated: April 2, 2025)

I. FIRST PRINCIPLES METHODS

In the following, we first describe our electronic structure calculations for paramagnetic Sr₂MgReO₆ (SMRO). We then proceed with the description of how the intersite exchange interaction (IEI) of the full effective Hamiltonian (5) are calculated on the basis of this electronic structure.

A. Correlated electronic structure calculations

The electronic structure of SMRO in the paramagnetic phase is computed using the DFT+dynamical mean-field theory (DFT+DMFT) method. The quantum impurity problem for the Re ion's *d* shell is solved within the quasi-atomic Hubbard-I (HI) approximation¹; we refer to this DFT+DMFT flavor as DFT+HI. We employ a fully charge self-consistent DFT+DMFT implementation^{2–4} based on the full-potential LAPW code Wien2k⁵, incorporating spin-orbit coupling via the standard variational treatment.

Wannier orbitals representing the Re *d* states are constructed from the manifold of *d* Kohn-Sham (KS) bands within the energy window [-1.36:5.44] eV relative to the KS Fermi level. The full *d*-shell parameters are set to $F^0 = U = 3.2$ eV and $J_H = 0.5$ eV, consistent with previous studies on *d*¹ and *d*² double perovskites (DP)^{6,7}.

The local density approximation (LDA) is used for the DFT exchange-correlation potential. Calculations are performed on a 300 \mathbf{k} -point mesh across the full Brillouin zone, with a Wien2k basis cutoff of $R_{mt}K_{max} = 7$. The double-counting correction is applied using the fully localized limit, assuming a nominal 5*d* shell occupancy of 1.

B. Calculation \mathbf{H}_{IEI}

We evaluate the IEI in SMRO using the force-theorem in the Hubbard-I (FT-HI) approach⁸, based on the converged electronic paramagnetic structure. This method accounts for small symmetry-breaking fluctuations in the density matrix of the ground-state (GS) $j_{eff} = 3/2$ multiplet, occurring simultaneously at two neighboring magnetic (Re) sites, *i* and *j*. The IEI, $V_{\Gamma\Gamma',\gamma\gamma'}^{KK'}(ij)$, is then determined by analyzing the response of the DFT+DMFT grand potential to these two-site fluctuations.

The FT-HI method parallels force-theorem techniques used for symmetry-broken magnetic states^{9,10} but is specifically formulated for the symmetry-unbroken paramagnetic state. Its application to SMRO closely follows previous implementations for $j_{eff} = 3/2$ double perovskites (DP)^{6,11}. A more detailed description can be found in the Appendix of Ref.¹¹ and the Supplementary Material of Ref.⁶, while the full derivation is presented in Ref.⁸.

Importantly, the reference frame for calculating IEI is the local octahedral frame of the main Figure 1b, rotated by an angle ϕ relative to the cubic crystallographic axis [100]. The dipole magnetic moments are then rotated by $45^\circ + \phi$ in order to compute them in the global reference frame.

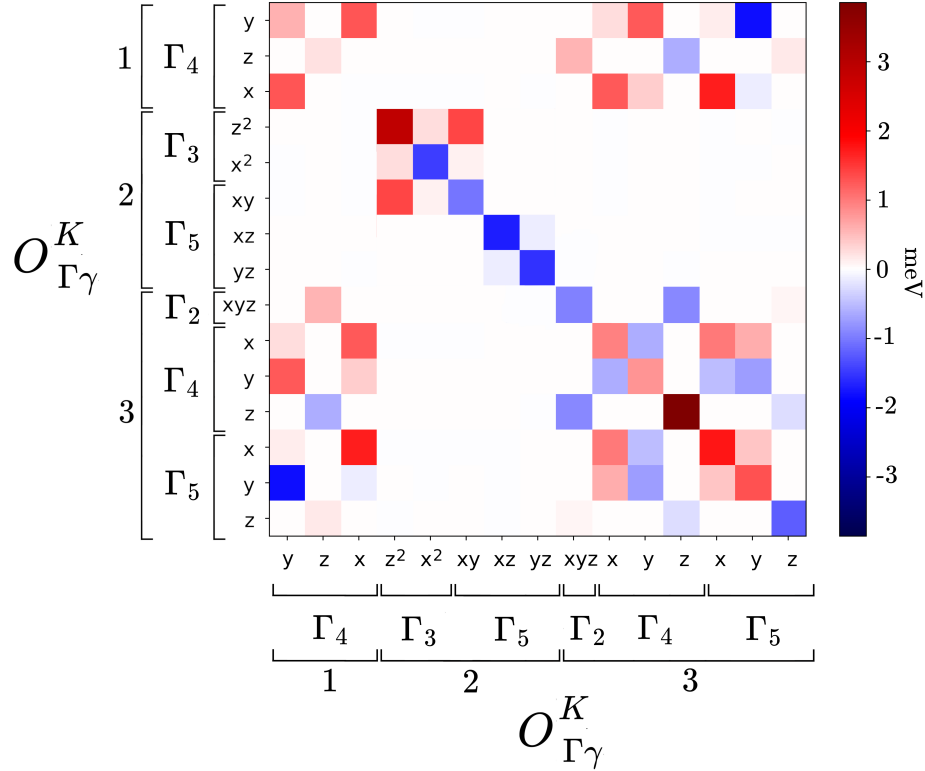
C. Calculations of neutron scattering

We evaluate the multipolar form-factors $F_\mu(\mathbf{q})$ for the Re⁶⁺ $j_{eff}=3/2$ manifold using the approach of Ref.⁷ and described in detail in the SM of that paper. The radial integrals of spherical Bessel functions $\langle j_L(k) \rangle$, $L = 0, 2, 4$ for Re⁶⁺ are taken from Ref.¹². The spherically averaged INS intensities are calculated for each $|\mathbf{q}|$ value by averaging over 642 \mathbf{q} points on an equidistributed icosahedral mesh.

II. INTERSITE EXCHANGE INTERACTIONS

In Suppl. Fig. 1 we plot the IEI of SMRO at room-temperature distortions as a color map; the IEI values are also listed in Suppl. Table I for two different – cubic and room-temperature distorted – lattice structures. The corresponding Hamiltonians (eq. 1 of the main text) have the canted- antiferromagnetic (cAFM) and anti-ferro octupolar (AFO) ground-state orders, respectively.

One may notice significant octupolar IEI, which are the largest couplings among time-odd IEI.



Supplementary Figure 1: Color map of the IEI $V_{\Gamma\Gamma',\gamma\gamma'}^{KK'}$ in SMRO of the for the $[1/2,1/2,0]$ Re-Re pair. All values are in meV. The numerical list of $V_{K\bar{K}'}^{QQ'}$ is given in Suppl. Table I.

Supplementary Table I: Calculated IEI $V_{\Gamma\Gamma',\gamma\gamma'}^{KK'}$ for the $j_{eff} = 3/2$ multiplet. First two columns list Γ and Γ' , respectively. Third and fourth column displays the γ and γ' components, respectively. The last three columns displays the values of IEI (in meV) for the [1/2,1/2,0] nearest-neighbor Re-Re bond in $\text{Sr}_2\text{MgReO}_6$ for the cubic non-distorted (Cubic) and experimental room-temperature tetragonal (RT-tetr) lattice structures respectively.

Γ	Γ'	γ	γ'	RT-tetr	Cubic
Dipole-Dipole					
Γ_4	Γ_4	y	y	0.58	0.59
Γ_4	Γ_4	y	x	1.27	1.49
Γ_4	Γ_4	z	z	0.22	0.23
Γ_4	Γ_4	x	x	-0.02	0.59
Quadrupole-Quadrupole					
Γ_3	Γ_3	z^2	z^2	2.87	3.71
Γ_3	Γ_3	z^2	x^2	0.25	0
Γ_3	Γ_5	z^2	xy	1.41	1.61
Γ_3	Γ_3	x^2	x^2	-1.46	-1.55
Γ_3	Γ_5	x^2	xy	0.10	0
Γ_5	Γ_5	xy	xy	-1.04	-1.00
Γ_5	Γ_5	xz	xz	-1.54	-1.70
Γ_5	Γ_5	xz	yz	-0.14	-0.19
Γ_5	Γ_5	yz	yz	-1.69	-1.70
Octupole-Octupole					
Γ_2	Γ_2	xyz	xyz	-0.94	-1.01
Γ_2	Γ_4	xyz	z	0.89	1.06
Γ_2	Γ_5	xyz	z	-0.07	0
Γ_4	Γ_4	x	x	0.95	1.10
Γ_4	Γ_4	x	y	-0.61	-0.69
Γ_4	Γ_5	x	x	1.00	1.22
Γ_4	Γ_5	x	y	0.61	0.65
Γ_4	Γ_4	y	y	0.81	1.10
Γ_4	Γ_5	y	x	-0.50	-0.65
Γ_4	Γ_5	y	y	-0.75	-1.22
Γ_4	Γ_4	z	z	3.85	4.90
Γ_4	Γ_5	z	z	-0.26	0
Γ_5	Γ_5	x	x	1.75	1.94
Γ_5	Γ_5	x	y	0.42	0.53
Γ_5	Γ_5	y	y	1.32	1.94
Γ_5	Γ_5	z	z	-1.21	-1.29
Dipole-Octupole					
Γ_4	Γ_4	y	x	0.25	0.32
Γ_4	Γ_4	y	y	1.24	1.56
Γ_4	Γ_5	y	x	0.15	0.19
Γ_4	Γ_5	y	y	-1.84	-2.20
Γ_4	Γ_2	z	xyz	-0.56	-0.59
Γ_4	Γ_4	z	z	-0.60	-0.86
Γ_4	Γ_5	z	z	0.16	0
Γ_4	Γ_4	x	x	1.25	1.56
Γ_4	Γ_4	x	y	0.37	0.32
Γ_4	Γ_5	x	x	1.69	2.20
Γ_4	Γ_5	x	y	-0.13	-0.19

III. PROJECTION OF $j_{eff}=3/2$ MULTIPOLAR OPERATORS INTO THE $m_j = \pm 3/2$ SPACE

The $|j_{eff} = 3/2, M\rangle$ basis of pseudo-spin-1/2 states for the $m_j = \pm 3/2$ ground-state doublet reads

$$|\uparrow\rangle = |3/2, 3/2\rangle; |\downarrow\rangle = |3/2, -3/2\rangle. \quad (1)$$

The resulting psudo-spin Hamiltonian is then related to the $j_{eff}=3/2$ one (eq. 1 of main text) by the projection

$$H_{E_g} = \hat{P} H_{IEI} \hat{P}^T = \sum_{\langle ij \rangle \in NN} \sum_{\alpha\beta} J_{\alpha\beta}(\Delta\mathbf{R}_{ij}) \tau_\alpha(\mathbf{R}_i) \tau_\beta(\mathbf{R}_j), \quad (2)$$

where the rows of projection matrix P are the $m_j = \pm 3/2$ states in $j_{eff} = 3/2$ basis, τ_α is the spin-1/2 operator for $\alpha = x, y$, or z .

Of the fifteen $j_{eff} = 3/2$ multipoles, only six have non-zero projection into the τ space; those projections expanded into the spin-1/2 operators are listed below. Namely, there is one dipole

$$O_{\Gamma_4,z}^1 \equiv J^z \rightarrow 2\sqrt{5}/5\tau_z,$$

three Γ_4 octupoles

$$O_{\Gamma_4,x}^3 \rightarrow \sqrt{5}/2\tau_x, \quad O_{\Gamma_4,y}^3 \rightarrow -\sqrt{5}/2\tau_y, \quad O_{\Gamma_4,z}^3 \rightarrow \sqrt{5}/5\tau_z.$$

as well as two Γ_5 octupoles

$$O_{\Gamma_5,x}^3 \rightarrow -\sqrt{3}/2\tau_x, \quad O_{\Gamma_5,y}^3 \rightarrow -\sqrt{3}/2\tau_y.$$

Of five quadrupolar operators, the O_{z^2} is mapped into the identity.

Substituting those expressions for the relevant multipoles into the effective Hamiltonian H_{eff} (eq. 1 of the main text) one may derive explicit formulas for the τ IEI in terms of the $j_{eff}=3/2$ IEI. For simplicity we will drop the Γ notation in $V_{\Gamma\Gamma',\gamma\gamma'}^{KK'}$ such that for example $V_{\Gamma_4\Gamma'_4,xx}^{33}$ reads $V_{44,xx}^{33}$.

We find that the diagonal terms are expressed as

$$J_{xx} = \frac{1}{4} \left[5V_{44,xx}^{33} + 3V_{55,xx}^{33} - 2\sqrt{15}V_{45,xx}^{33} \right], \quad (3)$$

$$J_{yy} = \frac{1}{4} \left[5V_{44,yy}^{33} + 3V_{55,yy}^{33} + 2\sqrt{15}V_{45,yy}^{33} \right], \quad (4)$$

$$J_{zz} = \frac{1}{5} \left[9V_{44,zz}^{11} + V_{44,zz}^{33} + 6V_{44,zz}^{31} \right]. \quad (5)$$

and off diagonal terms:

$$J_{xy} = \frac{1}{4} \left[-5V_{44,xy}^{33} - \sqrt{15}V_{45,xy}^{33} + 3V_{55,xy}^{33} + \sqrt{15}V_{54,xy}^{33} \right], \quad (6)$$

$$J_{xz} = \frac{1}{2} \left[V_{44,xz}^{33} + 3V_{44,xz}^{31} - \frac{\sqrt{15}}{5}V_{54,xz}^{33} - \frac{3\sqrt{15}}{5}V_{54,xx}^{31} \right], \quad (7)$$

$$J_{yz} = \frac{1}{2} \left[-V_{44,yz}^{33} - 3V_{44,yz}^{31} - \frac{\sqrt{15}}{5}V_{54,yz}^{33} - \frac{3\sqrt{15}}{5}V_{54,yz}^{31} \right] \quad (8)$$

The overall prefactors are due to different normalizations of the spin operators and the spherical tensors.

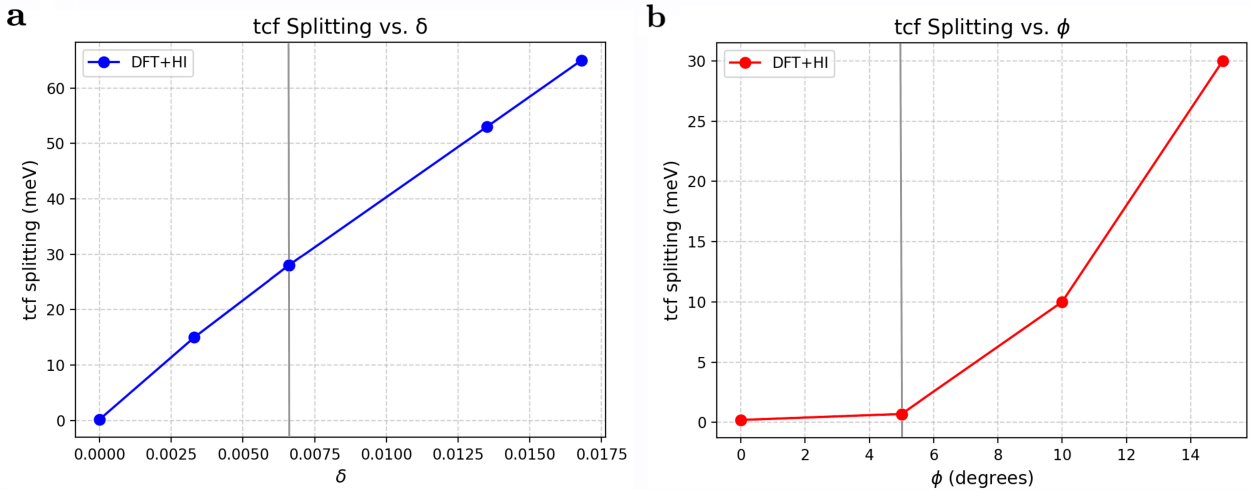
The final projected IEI are listed in Table II for the room-temperature tetragonal structure.

Supplementary Table II: Projected IEI for given lattice vectors.

$\mathbf{R} \in ab$ plane			$\mathbf{R} \in ac$ plane			$\mathbf{R} \in bc$ plane			
x	y	z	x	y	z	x	y	z	
x	0.55	0	0	4.48	0	0.05	4.51	0	-0.09
y	0	0.55	0	0	4.51	-0.09	0	4.48	-0.05
z	0	0	0.45	0.05	-0.09	2.73	-0.09	-0.05	2.73

IV. $j_{eff}=3/2$ SPLITTING AS FUNCTION OF δ, ϕ

The behavior of the $j_{eff}=3/2$ splitting is analyzed in two cases: 1) With fixed $\phi = 0^\circ$ angle by varying $\delta = c/(\sqrt{2}a) - 1$, where a and c are the lattice parameters of the tetragonal cell; 2) With fixed $\delta = 0$ by varying ϕ . The results are plotted in Figure 2 a and b respectively. Interestingly, while the tcf follows a linear behavior with varying δ , it grows instead exponentially with ϕ .



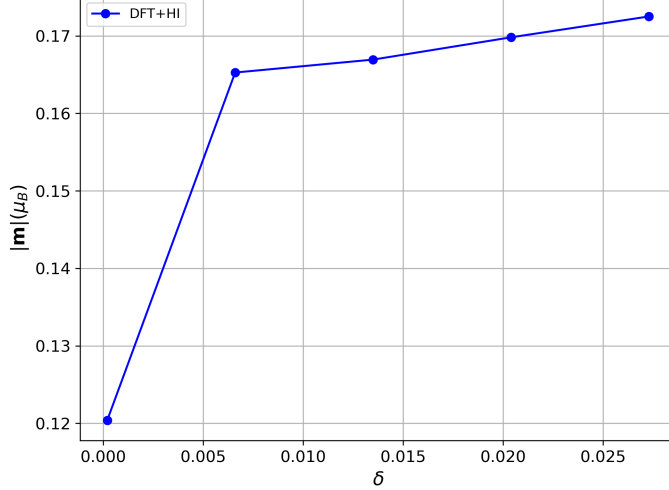
Supplementary Figure 2: a) $j_{eff}=3/2$ splitting for different values of $\delta = c/(\sqrt{2}a) - 1$ with fixed in-plane tilting angle $\phi = 0^\circ$. b) $j_{eff}=3/2$ splitting for different values of ϕ with fixed tetragonal distortion $\delta = 0$. The horizontal gray lines mark the room temperature experimental values.

V. MAGNETIC MOMENT DEPENDENCE WITH AS A FUNCTION OF tcf

The dependence of the magnetic moment on the tcf is presented in Figure 3. The observed increase in magnetic moment with tcf highlights the enhanced mixing between the $j = 3/2$ and $j = 1/2$ states, which consequently strengthens the dipole mixing within the AFO ground state.

Interestingly, in the cAFM phase at $\delta = 0$, the magnetic moment remains nonzero. This behavior arises directly from the choice of the Wannier projection window, which incorporates all d-orbitals. Including all d orbitals results in a small e_g contribution of ≈ 0.0043 within the $j = 3/2$ ground-state multiplet. Although minor, this mixing generates a significant magnetic moment of approximately $0.12 \mu_B$. This is a direct consequence of the interplay between a finite spin-orbit coupling and crystal field effect limits, as discussed by Stamokostas and coworkers¹³.

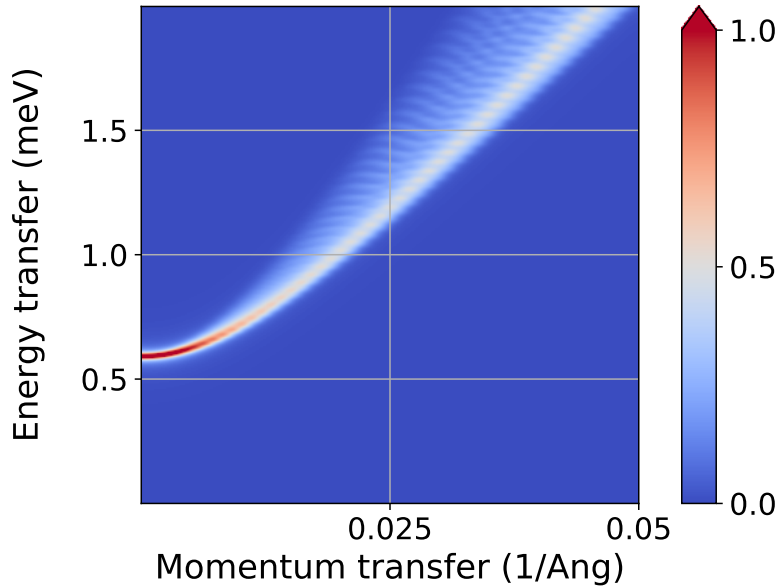
The disparity in magnitude between the $t_{2g} - e_g$ mixing and the total magnetic moment M_{tot} is well illustrated in Figure 4 of Ref.¹³.



Supplementary Figure 3: Modulus of Re magnetic moment as a function of the tcf $\delta = c/(\sqrt{2}a) - 1$.

VI. EXCITATION GAP IN THE AFO PHASE

In order to resolve the small excitation gap in the AFO case, which is not visible in Fig. 3b, we recalculated the INS intensity at small q and E using a dense mesh. The resulting spectra shown in Fig. 4 exhibits an excitation gap of 0.6 meV.



Supplementary Figure 4: INS intensity of the AF the small-energy-small- q INS intensity .

-
- ¹ J. Hubbard, “Electron correlations in narrow energy bands,” Proc. Roy. Soc. (London) **A 276**, 238 (1963).
- ² M. Aichhorn, L V. Pourovskii, V. Vildosola, M. Ferrero, O. Parcollet, T. Miyake, A. Georges, and S. Biermann, “Dynamical mean-field theory within an augmented plane-wave framework: Assessing electronic correlations in the iron pnictide LaFeAsO,” Phys. Rev. B **80**, 085101 (2009).
- ³ M. Aichhorn, L V. Pourovskii, and A Georges, “Importance of electronic correlations for structural and magnetic properties of the iron pnictide superconductor LaFeAsO,” Phys. Rev. B **84**, 054529 (2011).
- ⁴ M. Aichhorn, L V. Pourovskii, P. Seth, V. Vildosola, M. Zingl, O. E Peil, X. Deng, J. Mravlje, G. J Kraberger, C. Martins, *et al.*, “TRIQS/DFTTools: A TRIQS application for ab initio calculations of correlated materials,” Computer Physics Communications **204**, 200–208 (2016).
- ⁵ P Blaha, K Schwarz, G Madsen, D Kvasnicka, J Luitz, R Laskowski, F Tran, and L D. Marks, *WIEN2k, An augmented Plane Wave + Local Orbitals Program for Calculating Crystal Properties* (Karlheinz Schwarz, Techn. Universität Wien, Austria, ISBN 3-9501031-1-2, 2018).
- ⁶ D. Fiore Mosca, L V. Pourovskii, B. H. Kim, P. Liu, S. Sanna, F. Boscherini, S. Khmelevskyi, and C. Franchini, “Interplay between multipolar spin interactions, jahn-teller effect, and electronic correlation in a $J_{\text{eff}} = \frac{3}{2}$ insulator,” Phys. Rev. B **103**, 104401 (2021).
- ⁷ L V. Pourovskii, D. Fiore Mosca, and C. Franchini, “Ferro-octupolar order and low-energy excitations in d² double perovskites of osmium,” Phys. Rev. Lett. **127**, 237201 (2021).
- ⁸ L V. Pourovskii, “Two-site fluctuations and multipolar intersite exchange interactions in strongly correlated systems,” Phys. Rev. B **94**, 115117 (2016).
- ⁹ A.I. Liechtenstein, M.I. Katsnelson, V.P. Antropov, and V.A. Gubanov, “Local spin density functional approach to the theory of exchange interactions in ferromagnetic metals and alloys,” Journal of Magnetism and Magnetic Materials **67**, 65 – 74 (1987).
- ¹⁰ M. I. Katsnelson and A. I. Lichtenstein, “First-principles calculations of magnetic interactions in correlated systems,” Phys. Rev. B **61**, 8906–8912 (2000).
- ¹¹ L V. Pourovskii, “Multipolar interactions and magnetic excitation gap in d³ spin-orbit Mott insulators,” Phys. Rev. B **108**, 054436 (2023).
- ¹² Kohjiro Kobayashi, Tatsuya Nagao, and Masahisa Ito, “Radial integrals for the magnetic form factor of 5d transition elements,” Acta Crystallographica Section A **67**, 473–480 (2011).
- ¹³ Georgios L. Stamokostas and Gregory A. Fiete, “Mixing of t_{2g} – e_g orbitals in 4d and 5d transition metal oxides,” Phys. Rev. B **97**, 085150 (2018).